

Spitzer Reveals Hidden Quasar Nuclei in Some Powerful FR II Radio Galaxies

Patrick Ogle

Spitzer Science Center, California Institute of Technology, Mail Code 220-6, Pasadena, CA 91125

ogle@ipac.caltech.edu

David Whysong¹ & Robert Antonucci

Physics Dept., University of California, Santa Barbara, CA 93106

ABSTRACT

We present a *Spitzer* mid-infrared survey of 42 Fanaroff-Riley class II radio galaxies and quasars from the 3CRR catalog at redshift $z < 1$. All of the quasars and $45 \pm 12\%$ of the narrow-line radio galaxies have a mid-IR luminosity of $\nu L_\nu(15\mu\text{m}) > 8 \times 10^{43} \text{ erg s}^{-1}$, indicating strong thermal emission from hot dust in the active galactic nucleus. Our results demonstrate the power of *Spitzer* to unveil dust-obscured quasars. The ratio of *mid-IR luminous* narrow-line radio galaxies to quasars indicates a mean dust covering fraction of 0.56 ± 0.15 , assuming relatively isotropic emission. We analyze *Spitzer* spectra of the 14 mid-IR luminous narrow-line radio galaxies thought to host hidden quasar nuclei. Dust temperatures of 210-660 K are estimated from single-temperature blackbody fits to the low and high-frequency ends of the mid-IR bump. Most of the mid-IR luminous radio galaxies have a $9.7 \mu\text{m}$ silicate absorption trough with optical depth < 0.2 , attributed to dust in a molecular torus. Forbidden emission lines from high-ionization oxygen, neon, and sulfur indicate a source of far-UV photons in the hidden nucleus. However, we find that the other $55 \pm 13\%$ of narrow-line FR II radio galaxies are weak at $15 \mu\text{m}$, contrary to single-population unification schemes. Most of these galaxies are also weak at $30 \mu\text{m}$. Mid-IR weak radio galaxies may constitute a separate population of nonthermal, jet-dominated sources with low accretion power.

Subject headings: galaxies: active, galaxies: quasars, galaxies: jets, infrared: galaxies

¹now at NRAO, Array Operations Center, P. O. Box O, 1003 Lopezville Rd., Socorro, NM 87801-0387

1. Unification of Quasars and Radio Galaxies

The nature of the energy source in active galactic nuclei (AGNs) is a fundamental problem. The basic model attributes the large luminosity of these systems to gravitational energy release in an accretion disk around a supermassive black hole. A jet may be driven by magnetic fields threading the disk (Blandford & Payne 1982). The black hole spin energy may also be tapped and converted into electromagnetic Poynting flux and particles in a relativistic jet (Blandford & Znajek 1977; Punsly & Coroniti 1990; Meier 1999; De Villiers et al. 2004).

Extragalactic radio sources are categorized by their morphology as either of two types (Fanaroff & Riley 1974). Fanaroff-Riley (FR) type I sources are edge-darkened, while FR IIs are edge-brightened. The different morphology of FR Is indicates that they are not related to FR IIs by orientation. FR Is also have lower radio luminosities than FR IIs for a given host galaxy luminosity (Owen & Ledlow 1994; Bicknell 1996) and most have low-ionization nuclear emission region (LINER) spectra (Hine & Longair 1979). However, not all FR Is can be characterized by low accretion power (Whysong & Antonucci 2004; Cao & Rawlings 2004). The present paper focuses on FR IIs, which contain powerful jets with bright terminal hot spots and lobes. Furthermore, we count broad-line radio galaxies (BLRGs) as low-luminosity quasars.

Quasars and narrow-line radio galaxies (NLRGs) may be unified by orientation-dependent obscuration. Radio galaxies are thought to host quasar nuclei that are obscured by circum-nuclear dusty tori aligned with the radio jets (Antonucci 1984). Unification of radio galaxies and quasars can therefore explain the lack of quasars viewed at large angles to the radio axis (Barthel 1989). The percentage of high-redshift radio galaxies (60% of the 3CRR FR II sample at $z > 0.5$) would then indicate a torus covering fraction of ~ 0.6 .

However, there appears to be a discrepancy between the redshift distributions of quasars and radio galaxies at $z < 0.5$, with a factor of ~ 4 more narrow-line radio galaxies than quasars (Singal 1993). Furthermore, the median projected linear size of these 'excess' radio galaxies is smaller than expected for quasars seen in the sky plane (Singal 1993; Whysong 2005). The unification hypothesis may be modified to include a second population of lower luminosity, low-excitation FR II radio galaxies (Wall & Jackson 1997; Grimes, Rawlings, & Willott 2004). Alternatively, it has been argued that the torus covering fraction may increase with decreasing radio luminosity (Lawrence 1991).

The unification hypothesis has been qualitatively confirmed by spectropolarimetry of radio galaxies, many of which have been shown to have highly polarized broad emission lines and blue continuum, scattered from material which has a direct view of the active galactic

nucleus (Cimatti et al. 1997; Cohen et al. 1999). Of particular note are the original discovery of highly polarized broad $H\alpha$ from the hidden quasar nucleus in 3C 234 (Antonucci 1984), and the discovery of highly polarized broad $H\alpha$ in the spectrum of the powerful radio galaxy Cygnus A (Ogle et al. 1997). However, this method of detecting hidden quasars relies on an appropriately placed scattering region to view the otherwise hidden nucleus. Such a region is not guaranteed to exist for all radio galaxies, and thus spectropolarimetry can easily yield false negatives. Polarimetry is also ineffective at determining the luminosity of the hidden nucleus, since the scattering efficiency is usually unknown.

Another way to search for hidden quasar nuclei is to observe radio galaxies in the mid-IR. If the unification hypothesis is correct, the dusty torus should serve as a crude calorimeter of the central engine (Meisenheimer et al. 2001; Siebenmorgen et al. 2004; Haas et al. 2004; Whysong & Antonucci 2004). Optical, UV, and X-ray photons from the quasar nucleus are absorbed by dust in the torus and the energy is re-emitted in the thermal infrared. This explains why blue, UV color-selected quasars emit 10-50% of their luminosity in the IR (Sanders et al 1989; Haas et al. 2000). There appears to be no connection between the bulk of this IR emission and nonthermal radio emission, except in core-dominated radio sources such as blazars. Observations of matched 3CR quasars and radio galaxies by ISO indicate similar IR luminosities, consistent with the unification picture (Meisenheimer et al. 2001; Haas et al. 2004). However, differences in $24 \mu\text{m}/70 \mu\text{m}$ color may indicate that mid-IR emission from the torus is anisotropic by a factor of ≤ 3 (Shi et al. 2005).

We present *Spitzer* observations of a sample of 42 FR II radio galaxies and quasars selected from the 3CRR survey. The goals are to search for mid-IR emission from hidden quasar nuclei and test the ubiquity of the unification hypothesis. The *Spitzer* Infrared Spectrograph (IRS) combines the advantages of unprecedented sensitivity from $5\text{-}36.5 \mu\text{m}$ to measure the mid-IR continuum and spectral resolution to measure high ionization emission lines powered by hidden AGNs. In the current paper, we present evidence for hidden quasar nuclei based on mid-IR photometry extracted from the IRS spectra. We examine in detail the spectra of the subset of 14 mid-IR luminous radio galaxies which appear to contain hidden quasar nuclei. Spectra of the quasars and mid-IR weak radio galaxies and a statistical study of the complete sample will be presented in separate papers.

2. Sample

We begin by selecting a well-defined, radio flux-limited and redshift-limited sample of 55 radio galaxies and quasars from the 3CRR catalog (Laing, Riley, & Longair 1983). We

include all 3CRR sources with FR II radio morphology, a flux of $S_{178} > 16.4 \text{ Jy}^1$ at 178 MHz, and a redshift of $z < 1$. The original 3CRR catalog has a flux limit of 10 Jy at 178 MHz, is restricted to northern declinations ($\delta > 10^\circ$), and has galactic latitude $|b| > 10^\circ$. It is the canonical low-frequency selected catalog of bright radio sources, has optical identifications and redshifts for all entries, and has been extensively observed in most wavebands.

We select only sources with FR II radio morphology. We verify or update the FR classification of all sources by inspection of the latest published radio maps. Compact, steep-spectrum sources (CSSs: 3C 48, 138, 147, 286, and 309.1) with radio major axis $D < 10 \text{ kpc}$ (Fanti et al. 1985) are excluded from the sample because they may constitute a class of young or frustrated radio sources. Here and throughout this paper, we assume a cosmology with $H_0 = 70 \text{ km s}^{-1} \text{ Mpc}^{-1}$, $\Omega_m = 0.3$, and $\Omega_\Lambda = 0.7$. Size and morphology indicate that CSSs are not related to FR IIs by orientation.

It is essential for our unification studies that we select a sample based on isotropic radio lobe flux, and *not* on optical or IR properties, so that it is unbiased by orientation-dependent selection effects. In particular, our sample includes no blazars. No sources make the flux limit only because of beamed emission from the core of the radio jet. Our sample includes quasars as well as radio galaxies, and we use the quasar subsample as a control. We aim to determine whether and which narrow-line FR II radio galaxies have mid-IR power comparable to quasars or broad-line radio galaxies of similar radio lobe flux and redshift.

The 42/55 sources in our sample which we have observed with *Spitzer*, or which have *Spitzer* data in the public archive are listed in Tables 1 and 2. The 25 *mid-IR luminous* sources with $\nu L_\nu(15\mu\text{m}) > 8 \times 10^{43} \text{ erg s}^{-1}$ (14 NLRGs and 11 quasars or BLRGs) are listed in Table 1, and the 17 *mid-IR weak* galaxies with $\nu L_\nu(15\mu\text{m}) < 8 \times 10^{43} \text{ erg s}^{-1}$ are listed in Table 2. The reason for this particular division is explained below.

Optical source classifications are based on emission line properties. Type 1 sources have directly visible broad emission lines (quasars and BLRGs), and type 2 sources (NLRGs) do not. The NLRGs are further classified using their forbidden emission lines (Jackson & Rawlings 1997; Wilott et al. 1999)². High-excitation galaxies (HEGs) are defined to have [O III] $\lambda 5007$ equivalent widths of $> 10 \text{ \AA}$ and [O III] $\lambda 5007$ /[O II] $\lambda 3727 > 1$. The sources which do not meet these criteria are classified as low-excitation galaxies (LEGs). The equivalent width criterion ensures that [O III] is measurable in moderate S/N spectra. However, it

¹The radio flux limit is 15 Jy using Laing, Riley, & Longair (1983) flux values and 16.4 Jy on the standard Baars (1977) scale.

²Updated optical classifications are available at <http://www-astro.physics.ox.ac.uk/~cjlw/3crr/3crr.html>.

remains to be seen whether some sources with low [O III] equivalent width might have [O III] $\lambda 5007$ /[O II] $\lambda 3727 > 1$. In addition, we caution that [O II] and [O III] may be subject to differing amounts of extinction.

3. Observations

We observed the sources in our sample with the Infrared Spectrograph (IRS) on the *Spitzer* Space Telescope (Houck et al. 2004; Werner et al. 2004). We used the low-resolution ($R \sim 64 - 128$) modules Short-Low (SL) and Long-Low (LL) for accurate spectrophotometry over the wavelength range 5-36.5 μm . Wavelengths 36.5-40 μm are unusable because of low-S/N and 2nd-order bleed-through caused by filter delamination in LL 1st order (LL1). The absolute and relative flux accuracies of IRS are generally better than 10% and 4%, respectively, as judged from observations of bright standard stars. However, additional low-level instrumental artifacts may become important for faint sources.

We used IRS in standard flux-staring mode, for 2 cycles at 2 nod positions in each of the modules SL1, SL2 (SL 1st and 2nd order), and LL2 (LL 2nd order). We executed 1 cycle at 2 nod positions for LL1, which covers the 20-36.5 μm range. A typical observation includes 240 s of on-source exposure time in each of SL1, SL2, and LL1, and 480 s in LL2, for a total of 2000 s per target (including overhead). Archived IRS data are used for 14 sources which were observed partly or in full by other investigators (with similar or longer exposure times).

Nod or off-slit observations were subtracted to remove foreground emission from the telescope, zodiacal light, and interstellar medium. Spectra were then extracted from the Basic-Calibrated Datasets (BCDs), using the *Spitzer* IRS Custom Extraction (SPICE³ version 1.1) software and standard tapered extraction windows. The extraction window full-widths are proportional to wavelength in each order to match the diffraction-limited telescope point-spread function (SL2: 7".2 at 6 μm , SL1: 14".4 at 12 μm , LL2: 21".7 at 16 μm , LL1: 36".6 at 27 μm). We rebinned portions of the spectra of 3C 55, 172, 220.1, 244.1, 263.1, 280, and 330 by factors of 4-8 in order to improve the S/N at short wavelengths. Spectral orders were trimmed at the edges and merged to produce final spectra.

The SL and LL slits have widths of 3".7 and 10".6, respectively. Standard point-source flux calibrations (version 12.0) were applied to correct for slit and aperture losses and convert the spectra from electron s^{-1} to Jy. In most cases, fluxes match to $< 15\%$ across order boundaries, consistent with a point source that is well-centered in all of the slits. However,

³<http://ssc.spitzer.caltech.edu/postbcd/spice.html>

in 5 cases (3C 192, 216, 220.1, 380, and 381) SL2 fluxes are larger by 17-35% relative to the other orders. Assuming that these mismatches owe to variable slit-loss caused by pointing errors, the orders with low flux are adjusted upward to match the orders with high flux. Order mismatches may alternatively be an indication of extended mid-IR emission.

The results for a few sources with nearby neighbors in the slit should be viewed with caution. In the case of 3C 310, a nearby companion galaxy (to the east) may contribute a significant fraction of the flux ($< 50\%$) in the LL1 slit. Similarly, a nearby source may potentially contribute to the LL spectra of 3C 438 (which is, however undetected at $15 \mu\text{m}$). The SL2 spectrum of 3C 388 may be weakly affected by flux from a nearby star on the slit ($< 20\%$). The northern component of the double nucleus in 3C 401 falls outside of the SL slits, but falls inside the LL slit used to measure the $15 \mu\text{m}$ flux.

3.1. Mid-Infrared and Radio Luminosities

We measure the mean $6.5 - 7.5 \mu\text{m}$ and $13.0 - 17.0 \mu\text{m}$ flux densities F_ν (7 and $15 \mu\text{m}$, rest) of each target (Tables 1 & 2). All *Spitzer* flux densities in this paper are in observed units at a constant rest-frame wavelength defined by $\lambda_{\text{rest}} = \lambda_{\text{obs}}/(1+z)$, where z is the redshift measured from optical emission lines and cataloged in the NASA Extragalactic Database (NED⁴). This avoids any complication from potentially large cosmological K-corrections that could otherwise be introduced by a steep IR continuum slope or redshifted silicate absorption features.

We choose to measure the mid-IR flux at 7 and $15 \mu\text{m}$ to avoid the $9.7 \mu\text{m}$ trough and the deepest part of the $18 \mu\text{m}$ silicate absorption trough. We exclude the $14.0-14.5 \mu\text{m}$ and $15.3-15.8 \mu\text{m}$ wavelength regions from our photometry, to avoid emission from Ne V and Ne III. The 7 and $15 \mu\text{m}$ bands are within the *Spitzer* IRS bandpass for redshifts $z < 1.28$. However, the archival LL data for two quasars (3C 254 and 275.1) are not yet public. We extrapolate their SL spectra to obtain $F_\nu(15 \mu\text{m}, \text{rest})$ using $F_\nu(7 \mu\text{m}, \text{rest})$ and the observed (relatively line-free) 5-7 μm spectral index.

Radio luminosities $\nu L_\nu(178 \text{ MHz}, \text{rest})$ are estimated from the observed 178 MHz fluxes and K-corrected using the 178-750 MHz radio spectral index (Laing, Riley, & Longair 1983). The sources in our sample display a large range of nearly 3 orders of magnitude in mid-IR to radio luminosity: $\nu L_\nu(15 \mu\text{m})/\nu L_\nu(178 \text{ MHz}) = 0.8 - 680$ (Fig.1). This quantity is thought to reflect the relative importance of accretion luminosity and jet kinetic power dissipation.

⁴<http://nedwww.ipac.caltech.edu>

However, different size and time scales are probed by the radio (10 kpc-1 Mpc) and mid-IR (0.1-100 pc), and the radio power may be sensitive to differences in environmental conditions.

For the purpose of studying quasar and radio galaxy unification, it is natural to divide the sample into the *mid-IR luminous* NLRGs which emit as powerfully as quasars or BLRGs, and the *mid-IR weak* NLRGs that do not. We adopt an empirical dividing line of $\nu L_\nu(15 \mu\text{m}) > 8 \times 10^{43} \text{ erg s}^{-1}$ to separate hidden quasars from mid-IR weak radio galaxies. The cutoff is set at 1/2 the luminosity of the mid-IR weakest BLRG (3C 219) to allow for some degree of anisotropy at 15 μm . Fourteen NLRGs satisfy our criterion and are thus likely to contain hidden quasar or BLRG nuclei (Table 1). Notably, all of these NLRGs are optically classified as HEGs.

The 17 mid-IR weak NLRGs with $\nu L_\nu(15 \mu\text{m}) < 8 \times 10^{43} \text{ erg s}^{-1}$ (Table 2) have mixed optical classifications, including both HEGs and LEGs. These sources have lower S/N mid-IR spectra, which will be considered in detail in a later paper. Six mid-IR weak NLRGs (including 2 HEGs and 4 LEGs) are undetected by *Spitzer* at 15 μm , and one is also undetected at 7 μm .

3.2. Hidden Quasar Spectra

3.2.1. Continuum Emission

We now present *Spitzer* spectra of the 14 mid-IR luminous NLRGs that ostensibly contain hidden quasar nuclei (Figs. 2-4). We also plot the spectral energy distributions (SEDs) of the sources with published near-IR photometry (Fig. 5). The collected photometric data were measured in the J, H, K, L', and M wavelength bands from the ground (Lilly & Longair 1984; Lilly, Longair, & Miller 1985; Simpson, Rawlings, & Lacy 1999; Simpson & Rawlings 2000). The photometric apertures range in size from 3 – 11", with preference given to the apertures that most closely match the *Spitzer* SL slit width. Where available, the ground-based L' and M-band photometry agrees with *Spitzer* spectrophotometry remarkably well. There is no indication of variability over the time span of 20 yr.

Four of the low-redshift NLRGs (3C 33, 234, 381, and 452) have broad peaks in their νL_ν spectra (and SEDs) at $1.5 - 2.5 \times 10^{13} \text{ Hz}$ (12-20 μm). A maximum and spectral curvature near 20 μm are also suggestive of broad peaks in the *Spitzer* spectra of 3C 55, 244.1, 265, and 330. The large amplitude ($\sim 0.5 - 1.0 \text{ dex}$) of the mid-IR bump (Fig. 5) excludes a large contribution of synchrotron emission to the mid-IR continuum of most sources. This is not surprising if the equatorial plane of the dusty torus is roughly perpendicular to the radio jet, such that jet emission is beamed away. The high redshifts of the NLRGs 3C 172,

220.1, 263.1, 268.1, and 280 preclude the identification of a mid-IR bump in the SEDs of these sources. The unusually flat, blue SED of 3C 433 may indicate a quasar viewed at *low* inclination (Section 3.2.2).

We attribute the mid-IR continuum bump visible in most sources to thermal emission from warm or hot dust. Fitting the mid-IR peak with a single-temperature blackbody model indicates dust with a temperature of $210 - 225 \pm 0.5$ K (Fig. 5). While this temperature characterizes the peak of the mid-IR SED, hotter dust must also be present. At frequencies greater than the peak of the SED ($2.0 - 7.5 \times 10^{13}$ Hz), the continuum emission of most sources can be characterized using a power law with spectral index $\alpha = 1.1 - 2.1$ (Table 1 & Fig. 6). This emission likely comes from a continuous distribution of dust temperature. We measure the spectral index between 7 and 15 μm , avoiding the 9.7 μm and 18 μm silicate absorption troughs. The most blue and apparently hottest mid-IR luminous NLRG is 3C 265, while the most red and coolest are 3C 55 and 3C 268.1 (Fig. 6). In comparison, some mid-IR weak sources such as 3C 310 and 3C 388 are quite blue ($\alpha \sim -0.1 - +0.7$), indicating a large contribution of starlight from the host galaxy to the 7 μm continuum.

The near-IR continuum shifts into the *Spitzer* IRS passband for the highest redshift ($z > 0.7$) sources. The spectra of the NLRGs 3C 55 and 3C 265 steepen above 7.5×10^{13} Hz (below 4 μm). Fitting these spectral turnovers with single-temperature blackbodies, we find emission from hot dust with temperatures of 520 ± 10 K and 660 ± 10 K, respectively. Altogether, the mid-IR luminous radio galaxies in our sample show emission from dust with temperatures distributed in the range 210-660 K. Hotter temperature dust (up to the sublimation temperature) may be present but not visible for radio galaxy tori viewed at high inclination (Pier & Krolik 1992).

Extinction by cold foreground dust in the host galaxy may also affect the spectral index. For Galactic-type dust, $A(7, 15, 35 \mu\text{m})/A(V) = (0.020, 0.015, 0.004)$ (Mathis 2000). An extinction of $A(V) = 100$ would steepen the 7-15 μm spectral index by $\delta\alpha = 0.6$ (Fig. 6a). The observed range in spectral index for the mid-IR luminous NLRGs is $\delta\alpha = 1.0$, corresponding to $A(V, 7, 15, 35 \mu\text{m}) = (167, 3.3, 2.5, 0.6)$ mag. Thus if reddening by a cold foreground dust screen accounted entirely for the range in mid-IR slope, the mid-IR emission could be anisotropic by factors of $f_A(7, 15, 35 \mu\text{m}) \sim (22, 10, 1.3)$. However, these are upper limits since variations in the spectral index are also controlled by the physical temperature distribution of the visible dust.

The SEDs of several sources (3C 33, 55, 172, 265, and 452) have upturns at short wavelengths, which we attribute to stellar emission from the host galaxy (Fig. 5). The wavelength of the upturn (1-5 μm) is an indicator of the relative strength of the mid-IR bump seen from our direction vs. host galaxy light, occurring at shorter wavelength for sources

with a stronger mid-IR bump. This may have important consequences for understanding the K-z Hubble diagram for 3C radio galaxies, for which it has been argued that AGNs contribute a negligible fraction of the K-band flux (e.g., Simpson & Rawlings 2000). This may be incorrect for a few of the most luminous mid-IR sources in our sample, including 3C 234 and 3C 280 where there appears to be much emission from hot dust in the K band.

Detailed spectral modeling, combined with radio orientation indicators, promises to further characterize the temperature distribution, optical depth, and inclination of the dusty torus that is thought to produce most of the mid-IR emission from hidden quasar nuclei. Such an analysis is, however, outside the scope of the present paper.

3.2.2. Silicate Absorption

The silicate absorption trough at $9.7 \mu\text{m}$ is detected in 12/14 of the mid-IR luminous NLRG spectra (Table 3 & Figs. 2-4). The equivalent width $\text{EW}_{9.7}$ and apparent optical depth $\tau_{9.7}$ are measured relative to a local continuum fit to either side of the trough, indicated in Figures 2-4. The optical depth is averaged over the trough bottom (rest $9.2\text{-}10.2 \mu\text{m}$) to improve the S/N. It should be kept in mind that the apparent $\tau_{9.7}$ is just a convenient parameterization of (and lower limit to) the total optical depth since there must also be broad-band silicate absorption of the adjacent continuum.

The apparent silicate optical depths are small ($\tau_{9.7} = 0.02\text{--}0.2$), for all but 3C 55 and 3C 433. If attributed to foreground dust screens, this would indicate optical extinction of only $A_V = 0.2\text{--}5.1$ mag (Fig. 6b), assuming a Galactic extinction law with $A_V/\tau_{9.7} = 12.3\text{--}25.6$ mag (Rieke & Lebofsky 1985; Draine & Lee 1984). The extinction values are clearly underestimated since they imply that the hidden nuclei in 3C 234, 265, 381, and 452, which have $\tau_{9.7} \leq 0.1$, should be reddened but directly visible at $\text{H}\alpha$. The same discrepancy between $\tau_{9.7}$ and estimates of extinction at shorter wavelengths is seen for the hidden quasar nucleus in Cygnus A, and attributed to a radial gradient in torus dust temperature (Imanishi & Ueno 2000). The observed range of $\tau_{9.7}$ may correspond to a range of equatorial silicate dust column densities in the torus, or alternatively a range of viewing angles. In this regard, more detailed modeling of the torus, including its geometric and temperature structure is clearly called for.

Filling-in of the silicate troughs by silicate *emission* from the torus or narrow-line region (NLR) may also reduce the apparent silicate optical depths in some sources. This is predicted for an optically thick torus viewed at an intermediate or face-on inclination (Pier & Krolik 1992). Recently, strong silicate emission features were detected by *Spitzer* in several radio-

loud (3C) and radio quiet (PG) quasars (Siebenmorgen et al. 2005; Hao et al. 2005). The failure of previous attempts to observe this feature inspired torus models with large dust grain size (Laor & Draine 1993) or a spatial distribution of optically thick clumps (Nenkova, Ivezić, & Elitzur 2002). However, it appears that past non-detections owe to inadequate wavelength coverage to determine the underlying continuum.

The NLRGs 3C 55 and 3C 433 have significantly deeper silicate troughs than other NLRGs, with $\tau_{9.7} = 0.9$ and 0.7, respectively (Fig. 6b). We suggest that their active nuclei and tori are absorbed by an additional (kpc-scale) cold dust screen in the host galaxy. As noted above, the NLRG 3C 433 is unusual in having a flat, blue continuum (similar to some of the quasars in our sample). A blue mid-IR spectrum is not necessarily at odds with deep silicate absorption features. It can be understood if this is a quasar viewed at low inclination to the jet and torus axes, but through an ($A_V \sim 10$) cold dust screen. This amount of extinction would result in very little reddening at 7-15 μm ($\delta\alpha = 0.05 - 0.14$), but would be sufficient to create the deep 9.7 μm trough (Fig. 6b) and would obscure any optical broad lines.

The NLRG 3C 433 is also unique in having the only unambiguously detected 18 μm silicate trough, with equivalent width $EW_{18} = 0.42 \pm 0.01 \mu\text{m}$ and apparent optical depth $\tau_{18} = 0.07 \pm 0.03$ (averaged over 17-19 μm). The ratio of τ_{18} to $\tau_{9.7}$ apparent silicate trough depths is 0.10 ± 0.04 , consistent with a 0.11 ratio for Galactic-type silicate dust (Draine & Lee 1984). We do not see the full 18 μm silicate trough in the spectrum of 3C 55 because of inadequate rest-wavelength coverage.

3.2.3. *Forbidden Emission Lines*

All of the mid-IR luminous NLRGs with high S/N spectra have forbidden emission lines from highly ionized metals, including [O IV] $\lambda 25.89 \mu\text{m}$, [Ne II] $\lambda 12.81$, [Ne III] $\lambda 15.55$, [Ne V] $\lambda 14.3$, [Ne VI] $\lambda 24.31$, [Ne VII] $\lambda 7.65$, [S III] $\lambda 18.71$, [S III] $\lambda 33.48$, and [S IV] $\lambda 10.51$ (Figs. 2-4). We measure the line flux and rest equivalent width of each emission line relative to the local continuum level (Table 4). Formal uncertainties are computed from the noise in the continuum to either side of the line. Upper limits are estimated for undetected emission lines, assuming they are unresolved.

The large range of ionization states (especially high-ionization Ne V, Ne VI, and S IV) indicates photoionization by a hidden source of far-UV photons (Alexander et al. 1999; Sturm et al. 2002; Armus et al. 2004), e.g. a quasar nucleus. Low critical densities in the range $10^3 - 10^6 \text{ cm}^{-3}$ (Alexander et al. 1999) indicate that the forbidden lines arise in the

NLR. There could plausibly be contributions from starburst emission to the lower-ionization emission lines such as [Ne II]. For 3C 55 and 3C 433, the [S IV] $\lambda 10.51$ line has a relatively large flux even though it sits at the bottom of a deep silicate trough. This line must then arise from a region not heavily obscured by dust, such as the extended NLR. The resolving power of IRS is insufficient to measure the intrinsic emission line widths, which are therefore $< 4700 \text{ km s}^{-1}$.

In order to assess the ionization level of the emission line regions, we compute several emission line ratios (Fig. 7). In particular, the [O IV]/[Ne II] and [Ne V]/[Ne II] ratios can be used as diagnostics of the relative contributions of AGN and starburst emission to the mid-IR emission line spectra of galaxies (Genzel et al. 1998; Sturm et al. 2002). In the sources where O IV, Ne V, and Ne II emission are all detected (3C 33, 234, 381, and 433), we find [O IV] $\lambda 25.89 \mu\text{m}$ / [Ne II] $\lambda 12.81 \mu\text{m}$ > 1.0 (Fig. 7a) and [Ne V] $\lambda 14.3 /$ [Ne II] $\lambda 12.81 \mu\text{m}$ > 0.5 (Fig. 7c), indicating a $> 50\%$ AGN contribution to the emission line spectrum. The [Ne II] $\lambda 12.81 \mu\text{m}$ line is relatively weak or undetected in the $z > 0.2$ sources, making it difficult to apply these diagnostics. However, the large EWs of the [Ne VI] or [S IV] lines in 3C 55, 265, and 330 indicate that the emission line spectra of these sources are also AGN-dominated.

3.2.4. Molecular Emission

Polycyclic aromatic hydrocarbon (PAH) emission features are commonly seen in star-forming regions, starbursts, and starburst-dominated ULIRGs (e.g., Genzel et al. 1998; Armus et al. 2004). The only PAH feature we detect is the weak $11.3 \mu\text{m}$ line in the spectrum of 3C 33, with a flux of $2.3 \pm 0.3 \times 10^{-14} \text{ erg s}^{-1} \text{ cm}^{-2}$ and equivalent width of $0.009 \pm 0.003 \mu\text{m}$ (Fig. 2). We do not detect a $6.2 \mu\text{m}$ PAH feature in 3C 33 ($\text{EW} < 0.8 \mu\text{m}$) or any of the other mid-IR luminous NLRGs, though this spectral region is generally noisier. If present, we could not cleanly resolve the $7.7 \mu\text{m}$ PAH feature from the adjacent [Ne VI] line, nor the $12.7 \mu\text{m}$ PAH feature from the adjacent [Ne II] line. Regardless, we do not see any hint of these PAH features in any source, suggesting $\text{EW} \ll 0.1 \mu\text{m}$. Therefore in most cases, neither the 7.7 or $11.3 \mu\text{m}$ PAH features can have a significant impact on the measurement of the silicate trough.

The general lack of PAH features is a strong indication that the primary power source in mid-IR luminous radio galaxies is accretion power, not hot stars. It is likely that PAHs are destroyed in the torus, which is exposed to intense X-ray emission from the AGN (Voit 1991). The weak PAH emission that is present in 3C 33 may arise in star-forming regions shielded from the AGN.

We detect the H₂ 0-0 S(3) 9.67 μm and H₂ 0-0 S(1) 17.03 μm pure rotational emission lines of molecular hydrogen (at the 3σ level) only in the spectrum of the NLRG 3C 433 (Fig. 2). The line fluxes are $0.6 \pm 0.2 \times 10^{-14}$ and $1.4 \pm 0.4 \times 10^{-14}$ erg s⁻¹ cm⁻² respectively (EW = 0.008 and 0.013 μm). The location of the 9.67 μm line at the bottom the deep 9.7 μm silicate trough may indicate that the H₂ emission region is exterior to the obscuring dust screen. The H₂ emission lines can be produced in warm molecular gas heated either by shocks or X-ray photons from the AGN (Rigopoulou et al. 2002). The ratio of S(3)/S(1) line fluxes is 0.5 ± 0.2 , which indicates warm H₂ with an excitation temperature of 300 ± 30 K. We estimate a warm H₂ mass of roughly $2 \times 10^8 M_{\odot}$, assuming a Boltzmann distribution of rotational level populations, an unresolved source, and negligible mid-IR extinction.

4. Discussion

4.1. Hidden Quasar Nuclei

The high mid-IR luminosities $\nu L_{\nu}(15 \mu\text{m}) = 10^{44} - 10^{46}$ erg s⁻¹ of $45 \pm 12\%$ (14/31) of the FR II NLRGs in our sample are consistent with hidden quasar or BLRG nuclei. In fact, such copious hot dust emission directly requires a hidden source of quasar-like luminosity to power it. Including the 11 quasars and BLRGs seen directly, we find that at least $60 \pm 12\%$ (25/42) of 3CRR FR II sources at $z < 1$ with $S_{178} > 16.4$ Jy contain powerful AGNs.

The percentage of *mid-IR luminous* AGNs obscured by dust and therefore classified as NLRGs is $56 \pm 15\%$ (14/25), corresponding to a mean torus covering fraction of 0.56 and mean torus opening half-angle of $55 \pm 11^{\circ}$. (If the 8 mid-IR weak HEGs are counted as highly obscured quasars, then the mean torus covering fraction increases to 0.67 ± 0.14 .) Both of these numbers are consistent with the estimated 60% mean torus covering fraction required to unify $z = 0.5 - 1.0$ radio galaxies and quasars (Barthel 1989).

The receding torus model (Lawrence 1991) predicts a larger torus covering fraction for low luminosity sources. If so, we would expect a larger mean mid-IR/radio ratio and a smaller type 1 fraction for low-redshift than for high-redshift sources. The fraction of type 1 mid-IR luminous sources is 3/9 (0.3 ± 0.2) at $z < 0.5$ vs. 8/16 (0.5 ± 0.2) at $z > 0.5$. Clearly, a larger sample is needed to put meaningful constraints on the variation of torus covering fraction with redshift or luminosity.

For the galaxies that contain a powerful mid-IR source, we find that there are other indications of a hidden AGN. The high-ionization, mid-IR forbidden lines such as [Ne V], even more-so than the strong optical [O III] lines, are telltale signatures of a non-stellar source of FUV photons in the radio galaxies that show them. Because of the lower extinction in

the mid-IR relative to the optical, it is likely that we can see these lines closer to the nucleus than optical narrow lines such as [O III] (Haas et al. 2005).

At least three of the mid-IR luminous NLRGs in our sample are known to have highly polarized broad emission lines. The NLRG 3C 234 has quasar-like mid-IR luminosity and a highly polarized broad H α line (Antonucci 1984). The NLRG 3C 265 has quasar luminosity, highly polarized UV flux, and a highly polarized broad Mg II line (Tran et al. 1998). The low-redshift NLRG 3C 33 has mid-IR luminosity comparable to the BLRG 3C 219, and highly polarized broad H α and H β (Cohen et al. 1999). We have an ongoing program to obtain optical spectropolarimetry of the rest of the sources in our sample. While the radio galaxies with highly polarized broad lines are known to contain hidden type-1 AGNs, there were previously no reliable measurements of the hidden AGN luminosities. Our mid-IR flux measurements yield rough calorimetric estimates of the hidden AGN luminosities, subject to uncertainties in SED, torus covering fraction, and any mid-IR anisotropy.

4.2. Mid-IR Weak Radio Galaxies

The majority of radio galaxies in our sample (17/31 or $55 \pm 13\%$) are relatively weak mid-IR sources. It is possible that some of the AGNs are highly obscured even at 15 μm because they are viewed through a very large dust column. A mid-IR source obscured by a nearly Compton-thick ($\tau_e = 0.7$) disk with Galactic dust/gas ratio would have an equatorial extinction of ~ 5 mag (factor of 100) at 15 μm . Even in this case, any mid-IR emission above the disk might not be obscured. For example, there may be a contribution from dust in the narrow-line region (NLR), above the hole in the torus (e.g. NGC 1068, Galliano et al. 2005; Bock et al. 2000), tending to make the mid-IR emission more isotropic.

For galaxies with redshift $z \leq 0.22$, *Spitzer* can measure the flux at $\lambda = 30 \mu\text{m}$ (rest), which should be more isotropic and less subject to extinction than the 15 μm flux. Nevertheless, 9/11 mid-IR weak galaxies in this redshift range are also weak at 30 μm , with $\nu L_\nu(30 \mu\text{m}) < 8 \times 10^{43} \text{ erg s}^{-1}$. The two exceptions are 3C 61.1 and 3C 123, with $\nu L_\nu(30 \mu\text{m}) = 1.27 \pm 0.08$ and $1.4 \pm 0.2 \times 10^{44} \text{ erg s}^{-1}$, respectively. In comparison 3C 452, the weakest mid-IR luminous NLRG in this redshift range, has $\nu L_\nu(30 \mu\text{m}) = 8.63 \pm 0.09 \times 10^{43} \text{ erg s}^{-1}$. Therefore, reclassifying the NLRGs by their luminosity at 30 μm would only gain us an additional 2 mid-IR luminous sources. This leads us to believe that most of the mid-IR weak radio galaxies truly lack a powerful accretion disk. Relatively low accretion power suggests, but does not prove, that some FR II jets may be driven by radiatively inefficient accretion flows or black hole spin-energy (Begelman, Blandford, & Rees 1984; Meier 1999).

As we mentioned above, roughly half (9/17) of the mid-IR weak NLRGs are classified as LEGs with weak optical [O III] emission. The [O III] emission in these sources may be weak because there is no strong source of UV photons to power the NLR. Qualitatively similar conclusions have been drawn by other investigators (e.g., Hine & Longair 1979; Chiaberge et al. 2000; Grimes, Rawlings, & Willott 2004). Alternatively, the NLR may be partly or completely obscured in LEGs (Haas et al. 2005). It will be important to make a more quantitative assessment of the optical and IR emission line strengths, to evaluate the extinction and determine what UV luminosity is necessary to power the NLR in mid-IR weak NLRGs.

4.3. Radio Properties and Unification

One of the major motivations for the radio galaxy and quasar unification theory is the deficit of lobe-dominant vs. core-dominant FR II quasars (Barthel 1989). Relativistic beaming models predict that there should be relatively more sources where the radio jet is beamed away and the high frequency radio core is weak. Core fluxes at 5 GHz are tabulated for the 3CRR catalog by Laing et al. (2003)⁵. We identify the mid-IR luminous NLRGs in our sample with the missing lobe-dominant quasar population (Fig. 8). Their median core to lobe ratio is $R_c = \nu L_\nu(\text{core}, 5 \text{ GHz})/\nu L_\nu(178 \text{ MHz}) = 5$, while the median $R_c = 180$ for the quasars. Conversely, all of the mid-IR luminous sources with $R_c > 100$ are classified as quasars. We will perform a more detailed statistical analysis when the Spitzer observations of our full sample are complete.

For most mid-IR weak NLRGs, we reject the possibility that the AGN and radio core are viewed in an 'off' state while the radio lobes are still active. A 5 GHz core is detected in 13/17 of the mid-IR weak radio galaxies (Fig. 8) and 13/14 of the mid-IR luminous galaxies. Furthermore, mid-IR weak and mid-IR luminous NLRGs have comparable core to total luminosity ratios of $R_c = 1 - 100$. Deeper 5 GHz observations of the 5 non-detected cores (in 3C 28, 153, 172, 315, and 319) will be necessary to determine whether or not they are in an off state (e.g., $R_c < 0.1$).

We find that FR II radio morphology is not a reliable predictor of nuclear mid-IR luminosity for radio galaxies. *Contrary to the simple unification paradigm, not all narrow-line FR II galaxies host nuclei as powerful as quasars with matched radio lobe luminosity.* Unification theories must be modified to account for an additional population of mid-IR weak radio galaxies.

⁵The online 3CRR catalog is available at <http://www.3crr.dyndns.org>.

Both intrinsic jet power and interaction with the interstellar and intergalactic medium are likely to be important for determining radio morphology. The break luminosity between FR I and FR II radio sources is found to increase with host galaxy optical luminosity (Owen & Ledlow 1994; Bicknell 1996). The existence of radio sources with hybrid FR I/II morphology also points to the importance of environmental effects in determining radio morphology (Gopal-Krishna & Wiita 2000; Gawronski et al. 2005). Furthermore, most FR I radio jets are one-sided, relativistic, and narrowly collimated on sub-parsec scales, just like FR IIs, and decollimate only on kpc scales (e.g. M87, Junor, Biretta, & Livio 1999).

Contrary to a common misconception, not all FR I sources have radiatively inefficient nuclei. For example, Centaurus A is persuasively argued to have a powerful hidden AGN (Whysong & Antonucci 2004), and the BLRG 3C 120 is a well-known FR I source. Deep VLA observations of the optically luminous, 'radio-quiet' quasar E1821+643 demonstrate that it has an FR I radio morphology (Blundell & Rawlings 2001). These and other cases (Antonucci 2001) demonstrate that many powerful AGNs are FR Is.

The observed variation in radio morphology and a wide range in AGN radio-loudness (Kellerman et al. 1989) do not necessarily require a weak coupling between jet power and accretion power, but may demonstrate that multiple factors are at work. At least five parameters may be necessary to theoretically unify all AGN types: black hole mass, black hole spin, accretion rate, radiative efficiency, and viewing angle. There is still much work ahead before we completely understand how basic physical parameters regulate the activity of supermassive black hole systems. Models that tie jet production to accretion onto a spinning black hole are particularly promising (e.g., Meier 1999; Hawley & Krolik 2006).

Much progress has been made in understanding the aspect-dependent appearance of AGN disks and jets, as a consequence of relativistic beaming and obscuration (Urry & Padovani 1995). Our *Spitzer* observations confirm that many FR II radio galaxies would appear as powerful quasars if viewed from an unobscured direction (e.g. along the radio axis). However, just as many FR II radio galaxies would not. Our *Spitzer* observations also demonstrate that powerful radio jets may be produced even by mid-IR weak AGN. A powerful, luminous accretion disk is not always necessary to produce a highly collimated, relativistic jet.

5. Conclusions

(1.) We report on a large *Spitzer* spectroscopic survey of 3CRR FR II radio sources with $S_{178} > 16.4$ Jy at $z < 1$. We find strong mid-IR emission from $45 \pm 12\%$ (14/31)

of NLRGs, which have luminosities comparable to matched BLRGs and quasars. Other indicators including high-ionization mid-IR lines and highly polarized broad emission lines confirm that some of these sources contain hidden quasar or BLRG nuclei. This demonstrates the power of *Spitzer* IRS for unveiling hidden quasars and estimating their luminosities.

(2.) We present *Spitzer* spectra of the 14 mid-IR luminous radio galaxies. In most cases, the mid-IR continuum bump from 3-30 μm can be produced by a distribution of hot dust with temperatures in the range 210-660 K. These high temperatures are most likely maintained by hidden AGNs. The silicate absorption trough at 9.7 μm has an apparent optical depth of $\tau = 0 - 0.2$ in most cases, consistent with dust temperatures decreasing outward from the center of a dusty torus. Two sources, 3C 55 and 433, have deeper silicate troughs which may be produced by additional cool dust in the host galaxy.

(3.) However, not all FR II radio galaxies emit strongly in the mid-IR. Contrary to single-population unification schemes, the majority of narrow-line radio galaxies in our sample (17/31 or $55 \pm 13\%$) have weak or undetected mid-IR emission compared to matched quasars and BLRGs, with $\nu L_\nu(15 \mu\text{m}) < 8 \times 10^{43} \text{ erg s}^{-1}$. For a few sources, this may possibly be the result of anisotropic torus emission viewed through a large column density of dust. However, it is likely that most of the weakest sources do not contain a powerful accretion disk. These may be truly nonthermal, jet-dominated AGNs, where the jet is powered by a radiatively inefficient accretion flow or black hole spin-energy rather than energy extracted from an accretion disk.

This work is based on observations made with the *Spitzer* Space Telescope, which is operated by the Jet Propulsion Laboratory, California Institute of Technology under NASA contract 1407. We have also made use of the NASA/IPAC Extragalactic Database (NED) which is operated by the Jet Propulsion Laboratory, California Institute of Technology, under contract with NASA. Support for this research was provided by NASA through an award issued by JPL/Caltech. We thank Dave Meier, Lee Armus, Bill Reach, and the anonymous referee for their helpful input and comments on the manuscript.

REFERENCES

- Alexander, T., Sturm, E., Lutz, D., Sternberg, A., Netzer, H., & Genzel, R. 1999, ApJ, 512, 204
- Antonucci, R. R. J. 1984, ApJ 278, 499
- Antonucci, R. R. J. 2001, in Polarization Insights for Active Galactic Nuclei, Astrophysical

- Spectropolarimetry, ed. J. Trujillo-Bueno et al. (Cambridge: Cambridge University Press), astro-ph/0103048
- Armus et al. 2004, *ApJS*, 154, 178
- Baars, J. W. M., Genzel, R., Pauliny-Toth, I. I. K., & Witzel, A. 1977, *A&A*, 61, 99
- Barthel, P. D. 1989, *ApJ*, 336, 606
- Begelman, M. C., Blandford, R. D., & Rees, M. J. 1984, *Rev. Mod. Phys.* 56, 255
- Bicknell, G. V. 1996, in *Energy Transport in Radio Galaxies and Quasars*, ASP Conference Series 100, ed. P. E. Hardee, A. H. Bridle, and J. A. Zensus (San Francisco: ASP), 253
- Blandford, R. D., & Znajek, R. L. 1977, *MNRAS*, 179, 4338
- Blandford, R. D., & Payne, D. G. 1982, *MNRAS*, 199, 883
- Blundell, K. M. & Rawlings, S. 2001, *ApJ*, 562, L5
- Bock, J. J. et al. 2000, *AJ*, 120, 2904
- Cao, X. & Rawlings, S. 2004, *MNRAS*, 349, 1419
- Chiaberge, M., Capetti, A., & Celotti, A. 2000, *A&A* 355, 873
- Cimatti, A., Dey, A., van Breugel, W., Hurt, T., & Antonucci, R. 1997, *ApJ*, 476, 677
- Cohen, M. H., Ogle, P. M., Tran, H. D., Miller, J. S., & Goodrich, R. W. 1999, *AJ*, 118, 1963
- De Villiers, J.-P., Hawley, J. F., Krolik, J. H., & Hirose, S. 2005, *ApJ*, 620, 878
- Draine, B. T., & Lee, H. M. 1984, *ApJ*, 285, 89
- Fanaroff, B. L. & Riley, J. M. 1974, *MNRAS*, 167, 31
- Fanti, C., Fanti, R., Parma, P., Schilizzi, R. T., & van Breugel, W. J. M. 1985, *A&A*, 143, 292
- Galliano, E., Pantin, E., Alloin, D., & Lagage, P. O. 2005, *MNRAS*, 363, L1
- Gawronski, M. P., Marecki, A., Kunert-Bajraszewska, M. K., & Kus, A. J. 2005, *A&A*, in press, astro-ph/0509497

- Genzel, R. et al. 1998, *ApJ*, 498, 579
- Gopal-Krishna, & Wiita, P. J. 2000, *A&A*, 363, 507
- Grimes, J. A., Rawlings, S., & Willott, C. J. 2004, *MNRAS*, 349, 503
- Hao, L. et al. 2005, *ApJL*, 625, L75
- Haas, M., Muller, S. A. H., Chini, R., Meisenheimer, K., Klaas, U., Lemke, D., Kreysa, E., & Camenzind, M. *A&A* 2000, 354, 453
- Haas, M. et al. 2004, *A&A*, 424, 531
- Haas, M., Siebenmorgen, R., Schulz, B., Krugel, E., & Chini, R. 2005, *A&A*, 2005, 442, L39
- Hawley, J. F. & Krolik, J. 2006, *ApJ*, in press, astro-ph/0512227
- Hine, R. G. & Longair 1979, *MNRAS*, 188, 11
- Houck, J. et al. 2004, *ApJS*, 154, 18
- Imanishi, M. & Ueno, S. 2000, *ApJ*, 535, 626
- Jackson, N. & Rawlings, S. 1997, *MNRAS*, 286, 241
- Junor, W., Biretta, J. A., & Livio, M. 1999, *Nature*, 401, 891
- Kellerman, K. I., Sramek, R., Schmidt, M., Shaffer, D. B., & Green, R. 1989, *AJ*, 98, 1195
- Laing, R. A., Riley, J. M., & Longair, M. S. 1983, *MNRAS*, 204, 151
- Laing, R. A., Riley, J. M., Longair, M. S., Hardcastle, M., Leak, N., & Thomas, P. 2003, 'The online 3CRR catalog'
- Lacy, M., Rawlings, S., Hill, G. J., Bunker, A. J., Ridgway, S. E., & Stern, D. 1999, *MNRAS*, 308, 1096
- Laor, A. & Draine, B. T. 1993, *ApJ*, 402, 441
- Lawrence, A. 1991, *MNRAS*, 252, 586
- Lilly, S. J. & Longair, M. S. 1984, *MNRAS*, 211, 833
- Lilly, S. J., Longair, M. S., & Miller, L. 1985, *MNRAS*, 214, 109

- Mathis, J. S. 2000, in *Allen's Astrophysical Quantities*, 4th edition, ed. A. Cox (New York: Springer-Verlag), 523
- Meier, D. L. 1999, *ApJ*, 522, 753
- Meisenheimer, K., Haas, M., Mller, S. A. H., Chini, R., Klaas, U., & Lemke, D. 2001, *A&A*, 372, 719
- Nenkova, M., Ivezić, Z., & Elitzur, M. 2002, *ApJ*, 570, L9
- Ogle, P. M., Cohen, M. H., Miller, J. S., Tran, H. D., Goodrich, R. W., & Fosbury, R. A. E. 1997, *ApJ*, 482, L37
- Owen, F. N. & Ledlow, M. J. 1994, in *The First Stromlo Symposium: The Physics of Active Galaxies*, ASP Conference Series 54, ed. G. V. Bicknell, M. A. Dopita, & P. J. Quinn (San Francisco: ASP), 319
- Pier, E. A. & Krolik, J. H. 1992, *ApJ*, 401, 99
- Punsly, B. & Coroniti, F. V. 1990, *ApJ*, 354, 583
- Rieke, G. H. & Lebofsky, M. J. 1985, *ApJ*, 288, 618
- Rigopoulou, D., Kunze, D., Lutz, D., Genzel, R., & Moorwood, A. F. M. 2002, *A&A*, 389, 374
- Sanders, D. B., Phinney, E. S., Neugebauer, G., Soifer, B. T., & Matthews, K. 1989, *ApJ*, 347, 29
- Shi, Y. et al. 2005, *ApJ*, 629, 88
- Singal, A. K. 1993, *MNRAS*, 262, L27
- Siebenmorgen, R., Freudling, W., Krugel, E., & Haas, M. 2005, *A&A*, 421, 129
- Siebenmorgen, R., Haas, M., Krugel, E., & Schulz, B. 2005, *A&A*, 436, L5
- Simpson, C., Rawlings, S., & Lacy, M. 1999, *MNRAS*, 306, 828
- Simpson, C., Ward, M., & Wall, J. V. 2000, *MNRAS*, 319, 963
- Sturm, E. et al. 2002, *A&A*, 393, 821
- Tran, H. D., Cohen, M. H., Ogle, P. M., Goodrich, R. W., & di Serego Alighieri, S. 1998, *ApJ*, 500, 660

- Urry, M., & Padovani, P. 1995, *PASP*, 107, 803
- Voit, G. M. 1991, *ApJ*, 379, 122
- Wall, J. V. & Jackson, C. A. 1997, *MNRAS*, 290, L17
- Werner, M. et al. 2004, *ApJS*, 154, 1
- Whysong, D. H. 2005, PhD Thesis, University of California, Santa Barbara.
- Willott, C. J., Rawlings, S., Blundell, K. M., & Lacy, M. 1999, *MNRAS*, 309, 1017
- Whysong, D. H., & Antonucci, R. R. J. 2004, *ApJ*, 602, 116

Table 1. Mid-IR Luminous Sources

3C	type ^a	z	F_7^b	F_{15}^c	$\log \nu L_{15}^d$	α^e	S178 ^f
175	QSR	0.7700	6.96 ± 0.07	21.6 ± 0.7	45.83	1.49 ± 0.04	19.2
196	QSR	0.871	8.0 ± 0.1	22.9 ± 0.6	45.96	1.38 ± 0.04	74.3
216	QSR	0.6703	9.8 ± 0.1	28.7 ± 0.6	45.83	1.41 ± 0.03	22.0
219	BLRG	0.1744	3.6 ± 0.1	11.2 ± 0.4	44.21	1.50 ± 0.06	44.9
254	QSR	0.7361	6.02 ± 0.08	...	45.56:	...	21.7
263	QSR	0.646	13.6 ± 0.1	29.8 ± 0.8	45.81	1.03 ± 0.04	16.6
275.1	QSR	0.5551	3.04 ± 0.07	...	44.76:	...	19.9
325	QSR	0.8600	1.17 ± 0.07	4.1 ± 0.2	45.20	1.6 ± 0.1	17.0
380	QSR	0.6920	15.1 ± 0.1	40.4 ± 1.2	46.00	1.29 ± 0.04	64.7
382	BLRG	0.0579	86.1 ± 0.3	$114. \pm 2.$	44.24	0.37 ± 0.02	21.7
390.3	BLRG	0.0561	56.8 ± 0.5	$164. \pm 4.$	44.37	1.39 ± 0.03	51.8
33	HEG	0.0597	19.8 ± 0.3	$75. \pm 2.$	44.08	1.75 ± 0.04	59.3
55	HEG	0.7348	4.7 ± 0.1	23.3 ± 0.7	45.82	2.11 ± 0.06	23.4
172	HEG	0.5191	0.40 ± 0.04	1.5 ± 0.2	44.31	1.7 ± 0.2	16.5
220.1	HEG	0.610	0.77 ± 0.05	2.4 ± 0.1	44.67	1.5 ± 0.1	17.2
234	HEG ^g	0.1848	$86. \pm 2.$	$239. \pm 3.$	45.59	1.35 ± 0.03	34.2
244.1	HEG	0.4280	3.50 ± 0.09	14.4 ± 0.3	45.13	1.86 ± 0.04	22.1
263.1	HEG	0.8240	0.63 ± 0.07	2.7 ± 0.1	44.98	1.9 ± 0.2	19.8
265	HEG	0.8110	9.0 ± 0.1	21.1 ± 0.5	45.86	1.12 ± 0.04	21.2
268.1	HEG	0.970	< 0.5	3.0 ± 0.2	45.17	2.1 ± 0.2^h	23.3
280	HEG	0.996	4.58 ± 0.09	13.2 ± 0.4	45.83	1.39 ± 0.05	25.8
330	HEG	0.550	1.72 ± 0.06	6.4 ± 0.2	45.00	1.72 ± 0.06	30.3
381	HEG	0.1605	11.1 ± 0.2	36.4 ± 0.8	44.65	1.56 ± 0.05	18.1
433	HEG	0.1016	40.0 ± 0.4	$98. \pm 1.$	44.67	1.18 ± 0.02	61.3
452	HEG	0.0811	11.3 ± 0.2	$45. \pm 1.$	44.13	1.80 ± 0.04	59.3

^aOptical spectral type (Lacy et al. 1999; Jackson & Rawlings 1997).

^{b,c}Flux densities (mJy) and 3σ upper limits at $7 \mu\text{m}$ (rest) and $15 \mu\text{m}$ (rest) from *Spitzer* IRS.

^d Logarithm of luminosity (erg s^{-1}) at $15 \mu\text{m}$ (rest). Values for 3C 254 and 3C 275.1 are extrapolated from $7 \mu\text{m}$ because the LL data are unavailable.

^e Spectral power law index for $F_\nu \sim \nu^{-\alpha}$ from 7-15 μm (rest).

^f Radio flux density (Jy) at 178 MHz (observed) (Laing, Riley, & Longair 1983), multiplied by a factor of 1.09 to convert to the Baars (1977) standard flux scale.

^g The broad $\text{H}\alpha$ line visible in total flux is entirely scattered (Antonucci 1984).

^h Spectral power law index for 3C 268.1 measured from 8-15 μm (rest).

Table 2. Mid-IR Weak Sources

3C	type ^a	z	F_7^b	F_{15}^c	$\log \nu L_{15}^d$	α^e	S178 ^f
61.1	HEG	0.1878	0.64 ± 0.06	3.0 ± 0.2	43.70	2.0 ± 0.2	34.0
192	HEG	0.0597	1.28 ± 0.07	3.2 ± 0.2	42.71	1.2 ± 0.1	23.0
274.1	HEG	0.4220	0.20 ± 0.05	<0.9	<43.91	...	18.0
300	HEG	0.270	0.26 ± 0.04	0.7 ± 0.2	43.40	1.3 ± 0.4	19.5
315	HEG	0.1083	0.97 ± 0.08	1.9 ± 0.2	43.01	0.9 ± 0.2	19.4
388	HEG	0.0917	0.98 ± 0.06	0.84 ± 0.09	42.66	0.4 ± 0.2	26.8
436	HEG	0.2145	0.65 ± 0.05	1.5 ± 0.2	43.52	1.1 ± 0.2	19.4
438	HEG	0.290	0.16 ± 0.04	<0.45	<43.27	...	48.7
28	LEG	0.1953	0.45 ± 0.06	<0.30	<42.74	...	17.8
123	LEG	0.2177	1.07 ± 0.08	2.8 ± 0.4	43.81	0.7 ± 0.2	206.0
153	LEG	0.2769	0.29 ± 0.05	1.0 ± 0.2	43.59	1.7 ± 0.3	16.7
173.1	LEG	0.2921	0.38 ± 0.04	0.6 ± 0.1	43.40	0.6 ± 0.3	16.8
288	LEG	0.2460	0.40 ± 0.05	<0.60	<43.25	...	20.6
310	LEG	0.0538	0.81 ± 0.07	0.73 ± 0.1	41.98	-0.1 ± 0.2	60.1
319	LEG	0.1920	<0.15	<0.27	<42.68	...	16.7
326	LEG	0.0895	0.67 ± 0.09	<0.39	<42.16	...	22.2
401	LEG	0.2011	0.25 ± 0.05	0.8 ± 0.2	43.17	1.5 ± 0.4	22.8

^{a-f}See Table 1.

Table 3. Silicate Trough

3C	$EW_{9.7}^a$	$\tau_{9.7}^b$
33	-0.222 ± 0.007	0.14 ± 0.02
55	-1.51 ± 0.03	0.9 ± 0.1
172	> -0.4	...
220.1	> -0.3	...
234	-0.028 ± 0.006	0.019 ± 0.008
244.1	-0.23 ± 0.03	0.18 ± 0.08
263.1	-1.3 ± 0.2	...
265	-0.11 ± 0.03	0.04 ± 0.06
268.1	-0.4 ± 0.1	0.2 ± 0.5
280	-0.23 ± 0.02	0.16 ± 0.09
330	-0.41 ± 0.06	0.1 ± 0.1
381	-0.19 ± 0.02	0.07 ± 0.02
433	-1.30 ± 0.01	0.71 ± 0.07
452	-0.196 ± 0.009	0.10 ± 0.02

^aThe 9.7 μm silicate trough (rest) equivalent width in μm .

^bApparent 9.7 μm silicate optical depth, averaged over 9.2-10.2 μm (rest).

Table 4. Emission Lines^a

3C	[Ne VI] λ 7.65	[S IV] 10.51	[Ne II] 12.81	[Ne V] 14.3	[Ne III] 15.55	[S III] 18.71	[Ne V] 24.31	[O IV] 25.89
33	2.8(0.2) 0.022	1.2(0.1) 0.012	3.9(0.2) 0.037	2.0(0.3) 0.019	5.3(0.2) 0.051	2.5(0.4) 0.028	1.6(0.2) 0.029	8.1(0.2) 0.159
55	1.82(.06) 0.062	2.2(0.3) 0.17	< 0.5 < 0.01	1.1(0.2) 0.036	2.0(0.3) 0.068	< 0.4 < 0.01
172	< 0.1 < 0.08	< 0.2 < 0.1	< 0.3 < 0.08	< 0.6 < 0.2	< 0.6 < 0.2	< 0.8 < 0.3
220.1	< 0.2 < 0.06	0.5(0.2) 0.21	< 0.2 < 0.05	< 0.5 < 0.1	0.35(.09) 0.11	< 0.2 < 0.05
234	1.7(0.1) 0.0034	3.2(0.3) 0.0077	0.8(0.2) 0.0022	3.3(0.7) 0.010	8.2(0.7) 0.027	< 3. < 0.01	3.9(0.7) 0.026	7.5(1.0) 0.056
244.1	0.7(0.2) 0.033	0.9(0.2) 0.041	1.4(0.2) 0.067	0.6(0.4) 0.033	0.3(0.2) 0.02	0.68(.06) 0.043
263.1	< 0.6 < 0.1	< 0.8 < 0.3	0.6(0.2) 0.19	< 0.6 < 0.2	0.6(0.2) 0.23
265	0.6(0.2) 0.012	1.6(0.4) 0.040	< 0.8 < 0.02	< 0.6 < 0.02	< 0.5 < 0.02
268.1	0.49(.08) 0.15	< 0.4 < 0.1	< 0.4 < 0.1	< 0.8 < 0.4	< 0.2 < 0.04
280	< 0.3 < 0.01	< 0.5 < 0.02	0.3(0.1) 0.014	< 0.4 < 0.02	0.9(0.2) 0.050
330	0.4(0.2) 0.03	0.64(.08) 0.076	< 0.5 < 0.05	0.4(0.1) 0.04	0.7(0.2) 0.09	0.19(.08) 0.02
381	1.3(0.1) 0.019	0.62(.07) 0.012	0.6(0.2) 0.011	0.7(0.3) 0.014	1.2(.3) 0.025	1.49(.08) 0.040	0.56(.08) 0.026	3.9(0.2) 0.196
433	3.1(0.3) 0.014	2.2(0.2) 0.023	1.9(0.3) 0.012	2.7(0.3) 0.020	5.2(0.3) 0.042	1.2(0.8) 0.013	2.3(0.5) 0.028	7.9(0.4) 0.105
452	< 0.5 < .008	0.7(0.1) 0.012	2.11(.07) 0.034	< 0.3 < .005	1.9(0.2) 0.032	1.4(0.4) 0.026	< 0.3 < 0.01	1.3(0.2) 0.057

^aNotes. For each source, emission line fluxes (10^{-14} erg s⁻¹ cm⁻²) or 2σ upper limits are on the first line and rest equivalent widths (μm) are on the second line. Emission line rest wavelengths (μm) are at the top of each column.

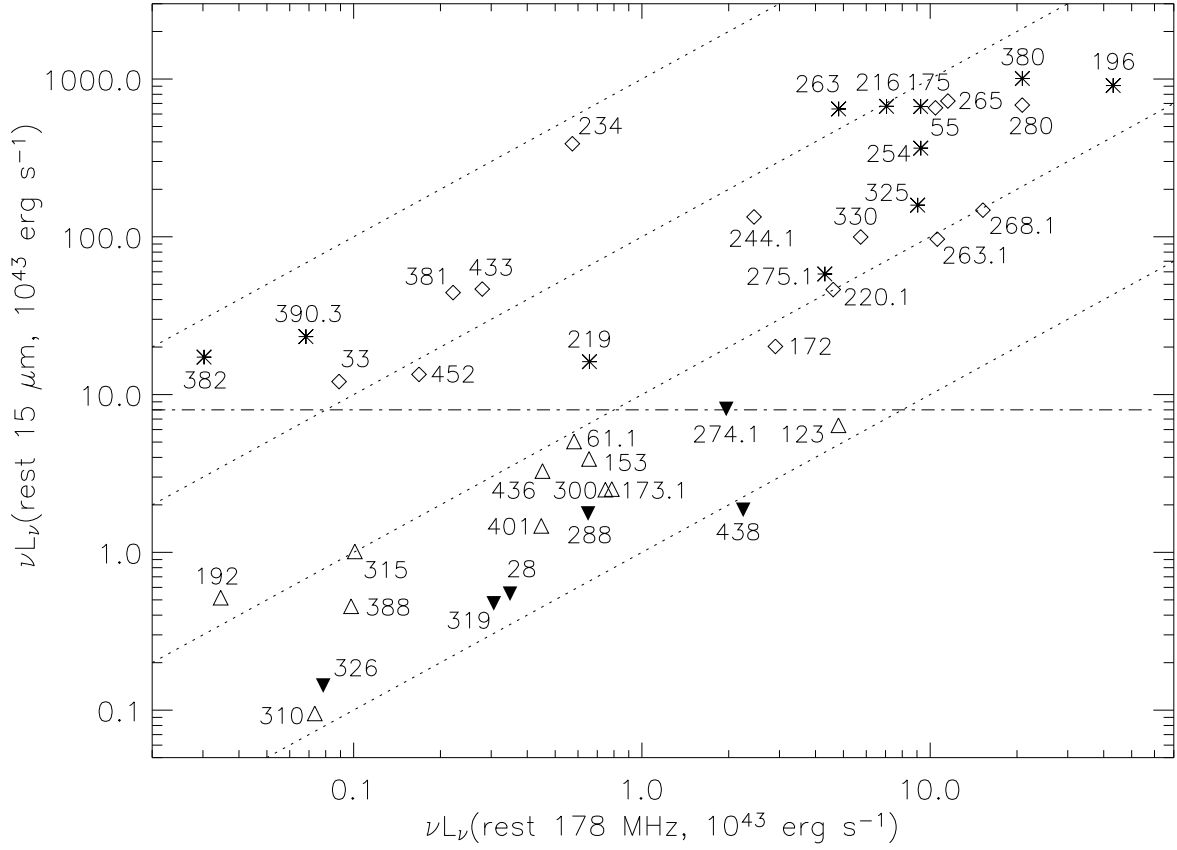


Fig. 1.— Comparison of 15 μm (rest) mid-IR power to 178 MHz (rest) radio power. The dotted lines indicate mid-IR to radio ratios of 1, 10, 100, and 1000. Quasars and BLRGs (asterisks) and mid-IR luminous NLRGs (diamonds) have mid-IR luminosities $\nu L_\nu(15\mu\text{m}) > 8 \times 10^{43} \text{ erg s}^{-1}$ (dot-dash line). Mid-IR weak NLRGs (open triangles) have $\nu L_\nu(15\mu\text{m}) < 8 \times 10^{43} \text{ erg s}^{-1}$. Filled triangles denote mid-IR weak NLRGs with 3σ upper detection limits at 15 μm .

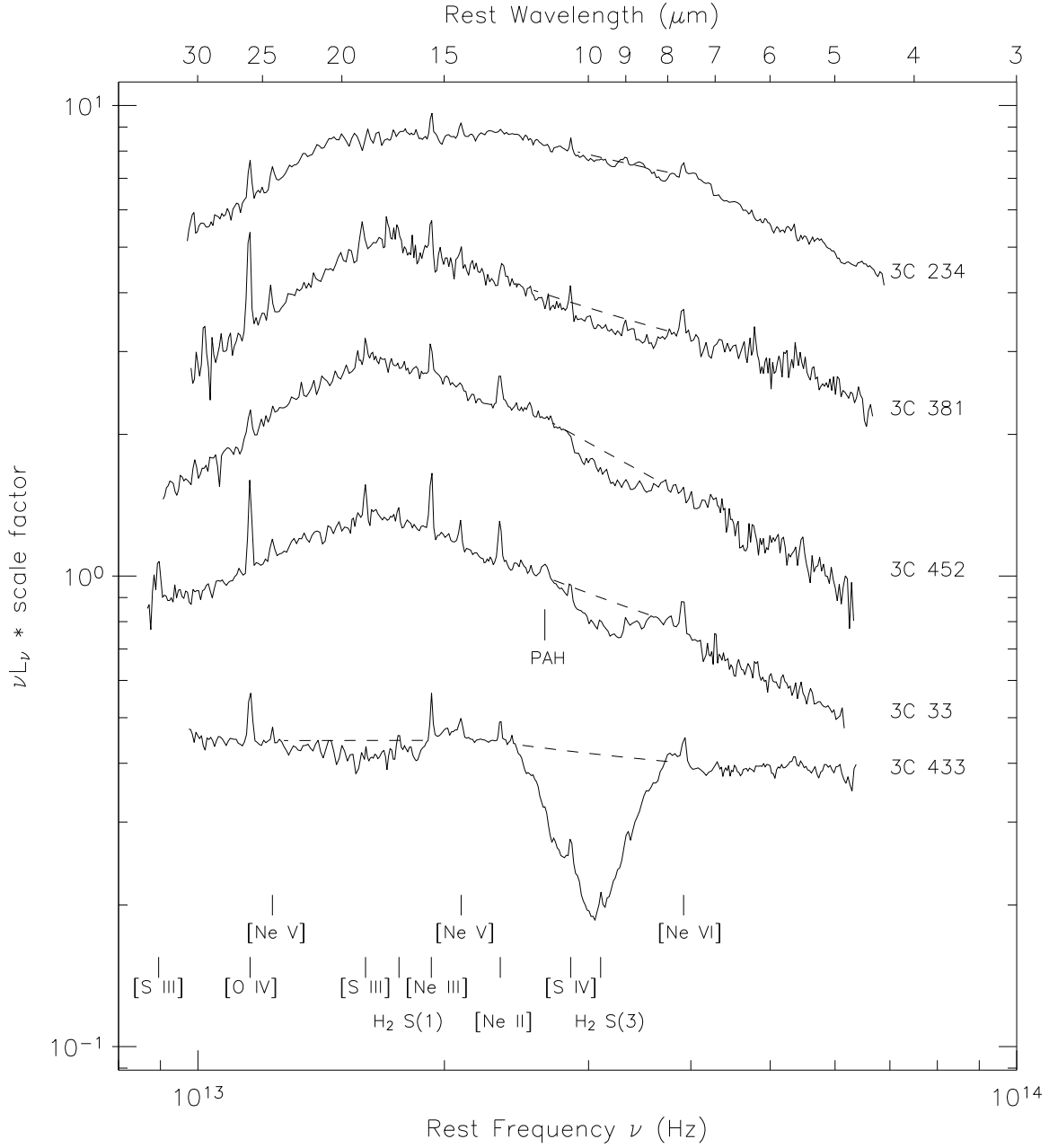


Fig. 2.— Spitzer spectra of mid-IR luminous narrow-line radio galaxies ($z = 0 - 0.2$), ordered by $9.7 \mu\text{m}$ silicate trough optical depth. The continuum fits used to measure the silicate troughs are shown as dashed lines. The peak at $12\text{-}20 \mu\text{m}$ is characteristic of thermal dust emission. Several high-ionization forbidden emission lines, H_2 pure rotational lines, and the $11.3 \mu\text{m}$ PAH feature are labeled.

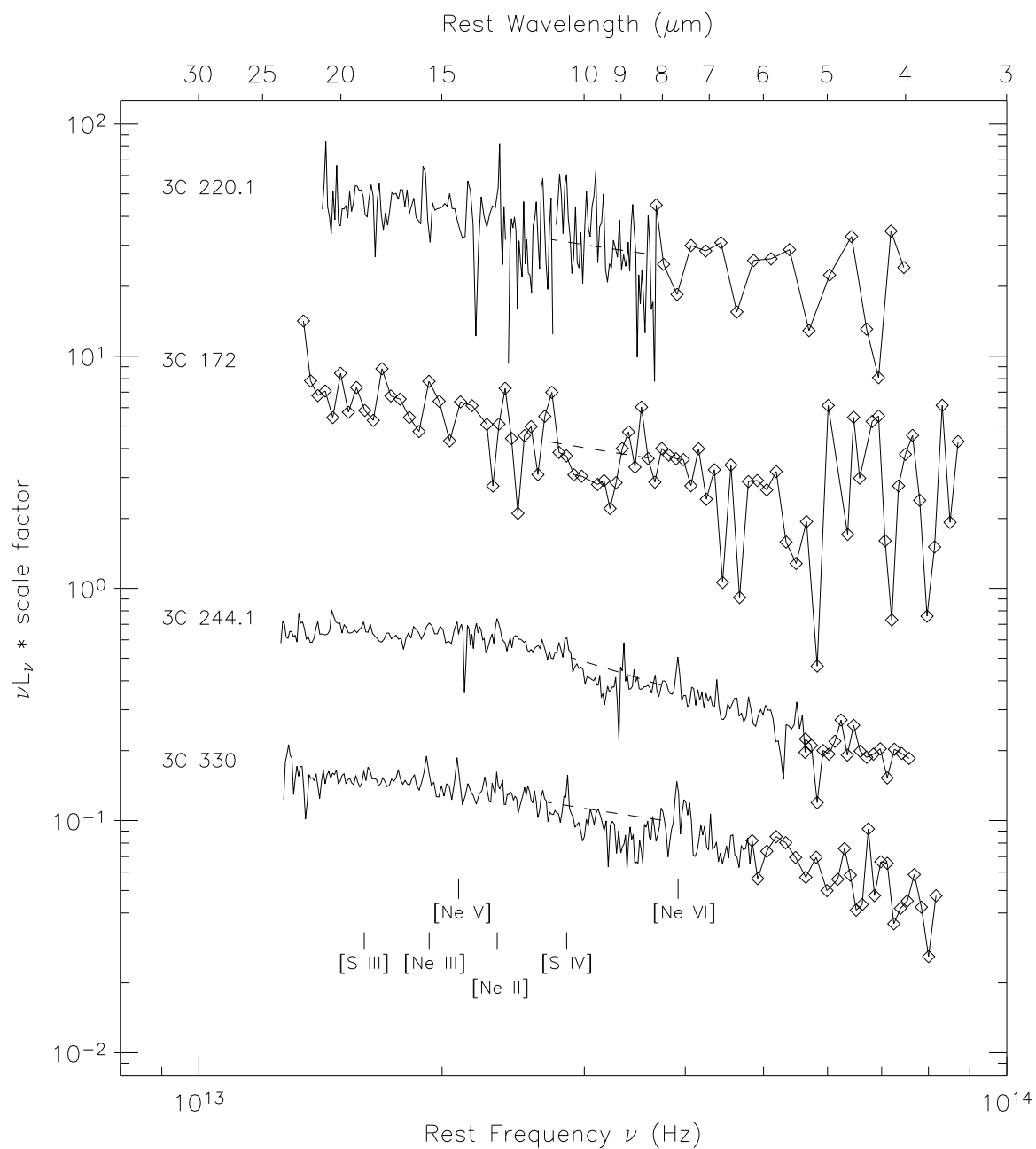


Fig. 3.— Spitzer spectra of mid-IR luminous NLRGs ($z = 0.2-0.7$). Some data are rebinned (diamonds) to improve S/N. Silicate absorption troughs (below dashed lines) and forbidden emission lines are present in some sources.

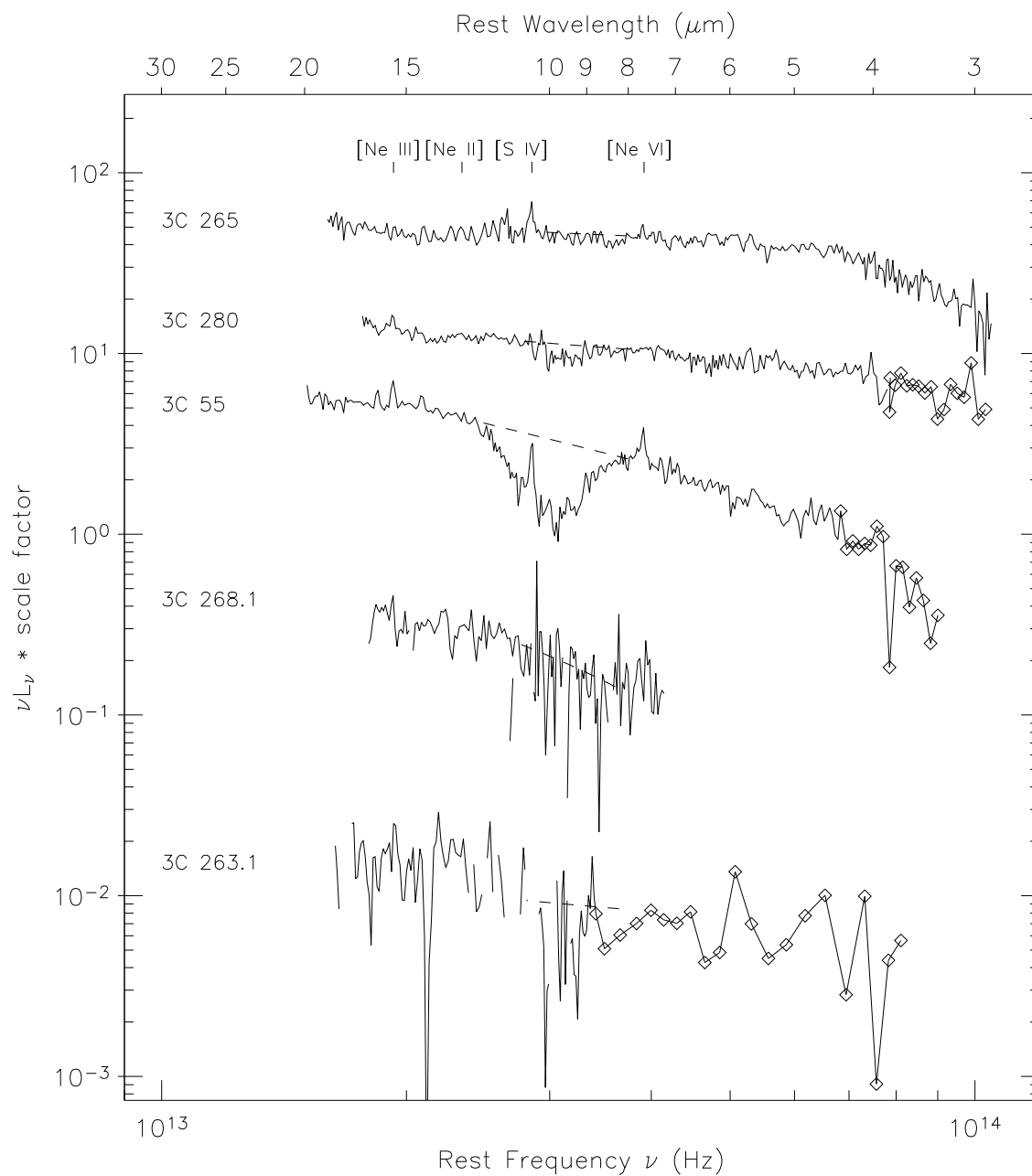


Fig. 4.— Spitzer spectra of mid-IR luminous NLRGs ($z = 0.7 - 1.0$). Some data are rebinned (diamonds) to improve S/N. Some of the large downward spikes and apparently missing data for 3C 263.1 and 268.1 are artifacts of plotting noisy data on a logarithmic scale. Silicate absorption troughs (below dashed lines) and forbidden emission lines are visible in some sources.

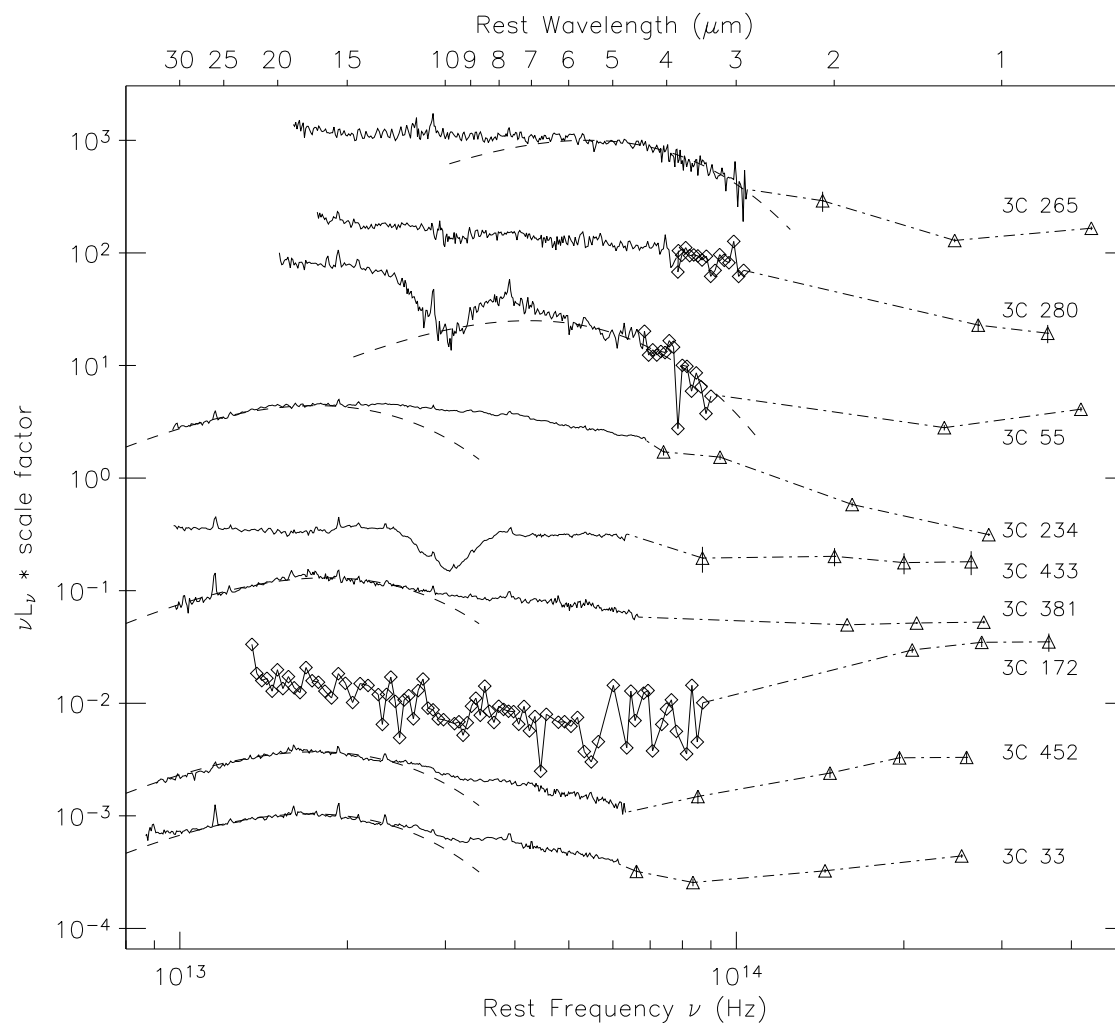


Fig. 5.— Spectral energy distributions of mid-IR-luminous NLRGs with near-IR photometry (triangles), ordered by $15 \mu\text{m}$ luminosity. *Spitzer* data (solid curves) reveal excess mid-IR emission relative to the near-IR stellar component. Blackbody fits (dashed curves) to the low and high-frequency ends of the *Spitzer* spectra indicate dust temperatures of 210-660 K.

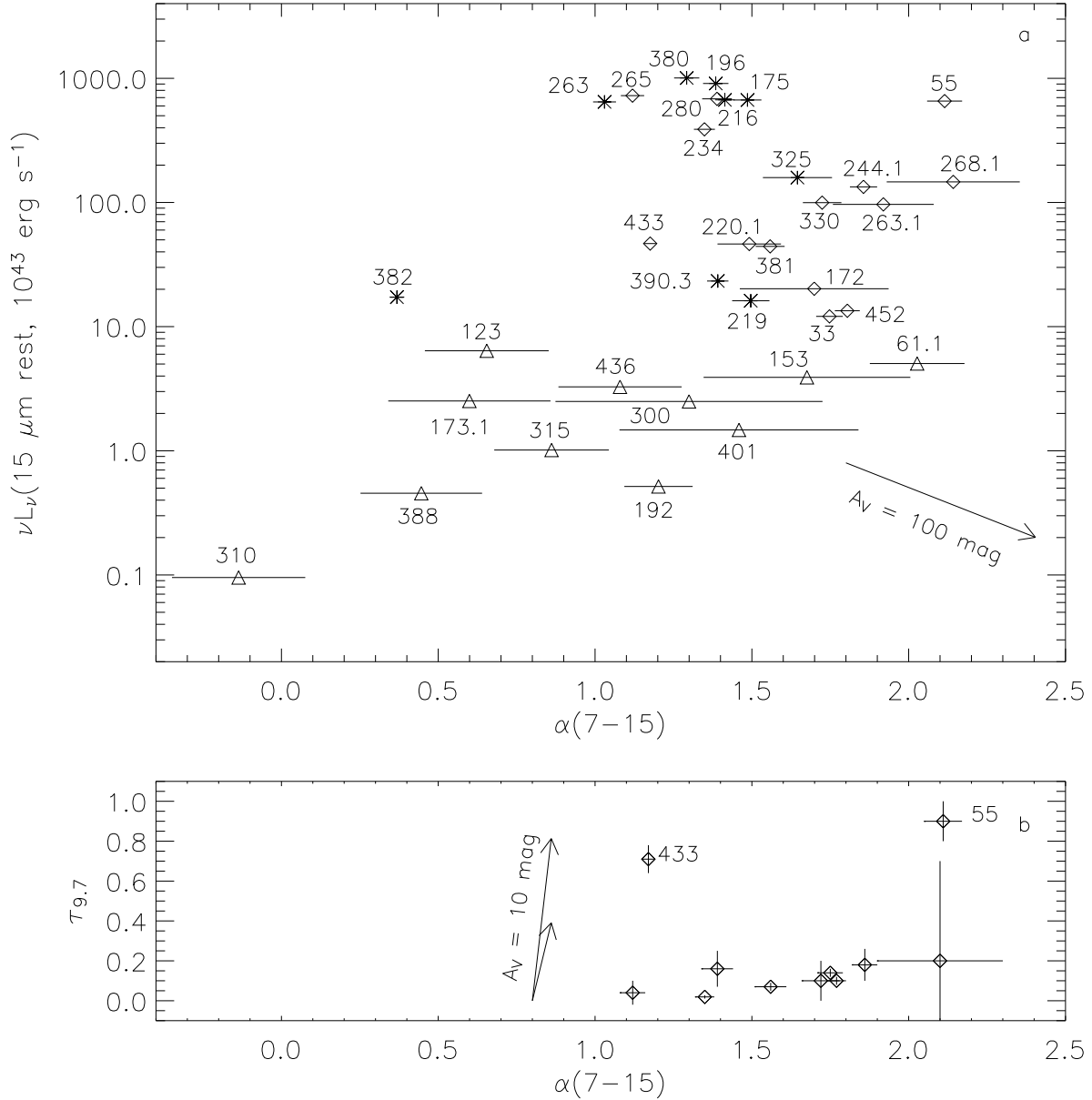


Fig. 6.— (a) Mid-IR luminosity vs. 7-15 μm spectral index for mid-IR luminous NLRGs (diamonds), mid-IR weak NLRGs (triangles), and quasars or BLRGs (asterisks). Mid-IR weak NLRGs with $\alpha < 1.0$ (e.g., 3C 310) have significant starlight from the host galaxy at 7 μm . The reddening vector corresponds to 100 magnitudes of optical (V band) extinction. (b) Silicate 9.7 μm apparent optical depth vs. 7-15 μm spectral index for mid-IR luminous NLRGs with well-measured troughs. The two reddening vectors both correspond to 10 magnitudes of optical (V band) extinction, for two different Galactic-type dust extinction curves (see text).

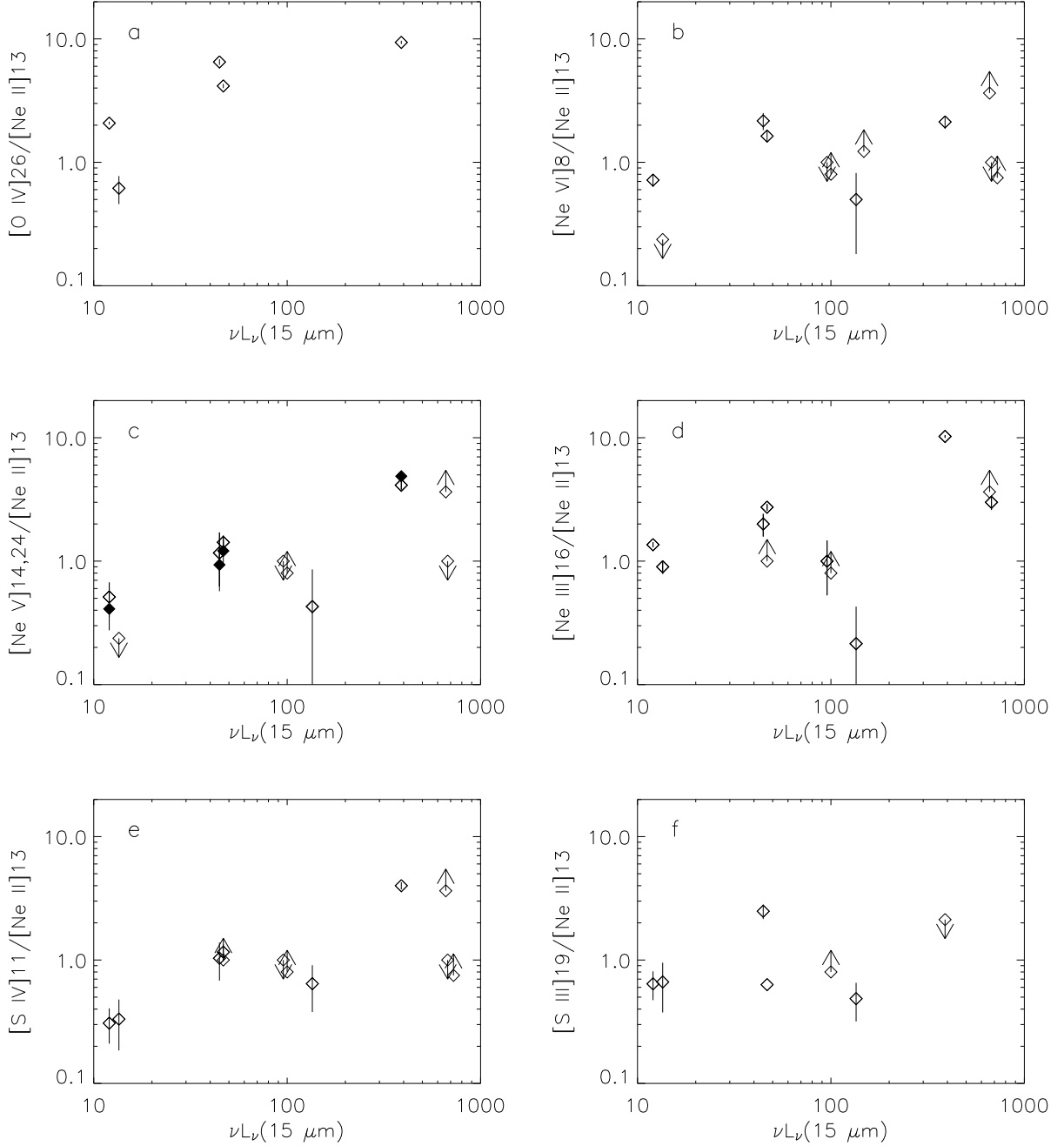


Fig. 7.— High-ionization emission line/ [Ne II] $\lambda 12.81 \mu\text{m}$ ratios vs. mid-IR luminosity $\nu L_{\nu}(15 \mu\text{m}, \text{rest})$ in units of $10^{43} \text{ erg s}^{-1}$, for mid-IR luminous NLRGs. (a) [O IV] $\lambda 25.89 \mu\text{m}$, (b) [Ne VI] $\lambda 7.65 \mu\text{m}$, (c) [Ne v] $\lambda 14.3 \mu\text{m}$ (open diamonds), and [Ne v] $\lambda 24.31 \mu\text{m}$ (filled diamonds), (d) [Ne III] $\lambda 15.55 \mu\text{m}$, (e) [S IV] $\lambda 10.51 \mu\text{m}$, and (f) [S III] $\lambda 18.71 \mu\text{m}$.

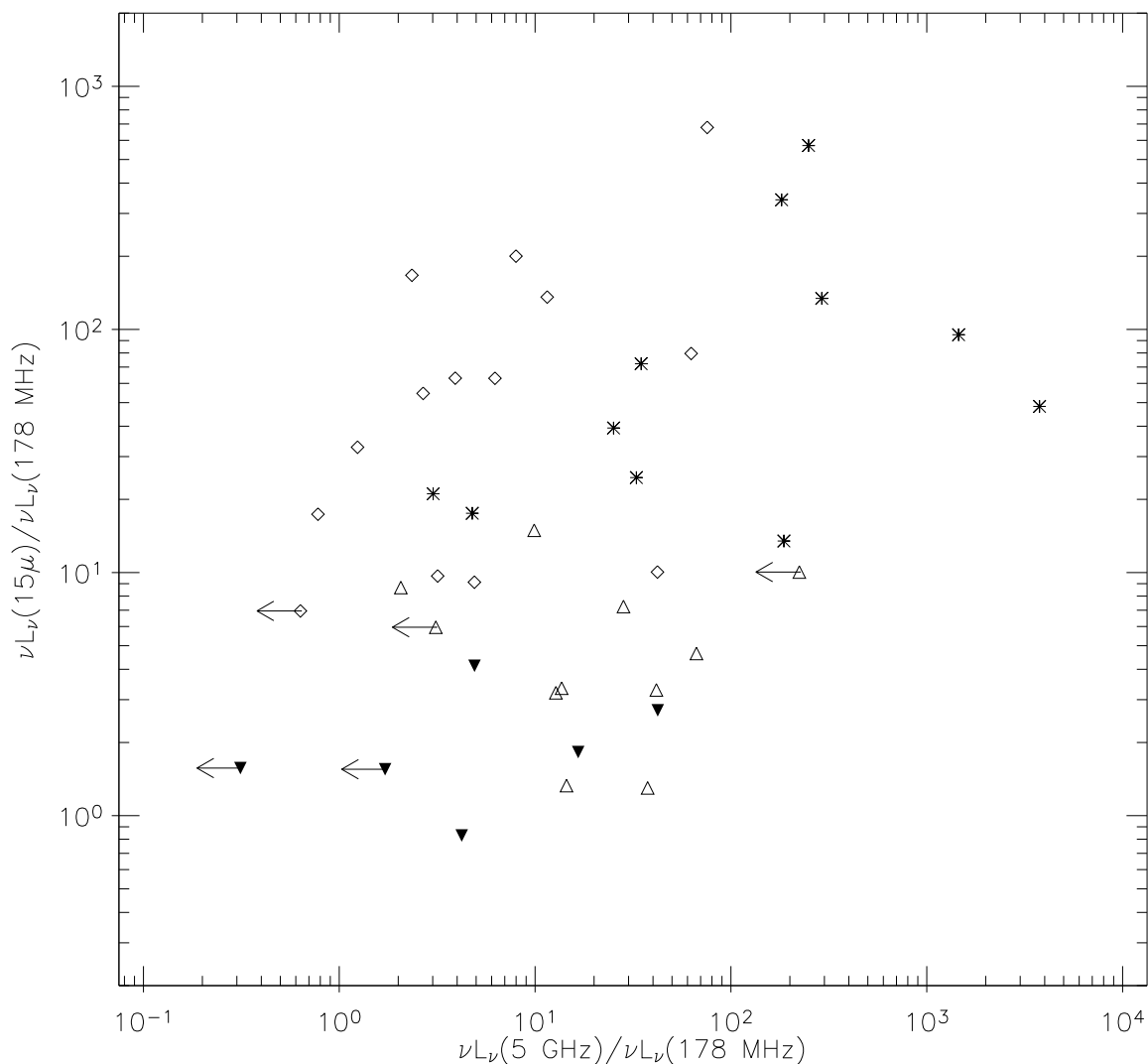


Fig. 8.— Mid-IR ($15\mu\text{m}$, rest) luminosity vs. 5 GHz (observed) radio core luminosity, both normalized by 178 MHz (rest) radio lobe luminosity. The various symbols represent mid-IR weak NLRGs (triangles, filled = upper limit), mid-IR luminous NLRGs (diamonds), and quasars (asterisks). Upper limits at 5 GHz are indicated by arrows. The most core-dominant sources, with $\nu L_\nu(5 \text{ GHz})/\nu L_\nu(178 \text{ MHz}) > 10^2$ are all quasars or BLRGs.